Title
Prp8 impacts cryptic but not alternative splicing frequency

Journal
Proceedings of the National Academy of Sciences of the United States of America, 116(6)

ISSN
0027-8424

Authors
Mayerle, Megan
Yitiz, Samira
Soulette, Cameron
et al.

Publication Date
2019-02-05

DOI
10.1073/pnas.1819020116

Peer reviewed

Prp8 impacts cryptic but not alternative splicing frequency

Megan Mayerle[a,1], Samira Yitiz[b], Cameron Soulette[b], Lucero E. Rogel[b], Andrea Ramirez[b], J. Matthew Ragle[b], Sol Katzman[c], Christine Guthrie[a,2], and Alan M. Zahler[b,2]

[a]Department of Biochemistry and Biophysics, University of California, San Francisco, CA 94143; [b]Department of Molecular, Cellular, and Developmental Biology and Center for Molecular Biology of RNA, University of California, Santa Cruz, CA 95064; and [c]Center for Biomolecular Science and Engineering, University of California, Santa Cruz, CA 95064

Contributed by Christine Guthrie, December 12, 2018 (sent for review November 7, 2018; reviewed by Marlene Belfort and Gideon Dreyfuss)

Pre-mRNA splicing must occur with extremely high fidelity. Spliceosomes assemble onto pre-mRNA guided by specific sequences (5′ splice site, 3′ splice site, and branchpoint). When splice sites are mutated, as in many hereditary diseases, the spliceosome can aberrantly select nearby pseudo- or "cryptic" splice sites, often resulting in nonfunctional protein. How the spliceosome distinguishes authentic splice sites from cryptic splice sites is poorly understood. We performed a *Caenorhabditis elegans* genetic screen to find cellular factors that affect the frequency with which the spliceosome uses cryptic splice sites and identified two alleles in core spliceosome component Prp8 that alter cryptic splicing frequency. Subsequent complementary genetic and structural analyses in yeast implicate these alleles in the stability of the spliceosome's catalytic core. However, despite a clear effect on cryptic splicing, high-throughput mRNA sequencing of these *prp-8* mutant *C. elegans* reveals that overall alternative splicing patterns are relatively unchanged. Our data suggest the spliceosome evolved intrinsic mechanisms to reduce the occurrence of cryptic splicing and that these mechanisms are distinct from those that impact alternative splicing.

cryptic splicing | alternative splicing | spliceosome | PRP8 | CRISPR mutagenesis

Splicing is an essential step in gene expression. The spliceosome, a large, RNA-based molecular machine, identifies and catalyzes the removal of noncoding introns and joining of flanking coding exons of pre-mRNAs (1). Splicing is an inherently high-fidelity process, and errors in splicing have been linked to many human diseases (2). Introns contain specific consensus sequences at their 5′ and 3′ ends (5′ and 3′ splice sites, SSs) as well as at an internal branchpoint. The spliceosome recognizes and binds to these sequences, and proper SS recognition by the spliceosome is required for high-fidelity pre-mRNA splicing (1).

During cryptic splicing, the spliceosome selects a sequence element that resembles, but is not, a bona fide SS. This often occurs when a true SS has been mutated and nearby cryptic sites, usually defined by a 5′ GU or a 3′ AG, are selected. Use of a cryptic site can result in changes to a gene's ORF and consequent disruption of gene expression. A small subset of core splicing factors have been implicated in cryptic splicing (3–5).

During assembly, the spliceosome undergoes considerable conformational rearrangements (1). Prp8 is the largest and most highly conserved protein in the spliceosome and has been directly implicated in splicing fidelity (6). The bulk of Prp8 surrounds and stabilizes the spliceosome's catalytic core, contacting the catalytic U6 snRNA and pre-mRNA substrate (7, 8). One key rearrangement is the closure of the spliceosome's catalytic core. In catalytic core closure, Prp8's N-terminal and large domains come into close proximity, helping to organize and support the snRNAs and pre-mRNA for catalysis (9–13). There is evidence that the spliceosome's catalytic core opens and closes repeatedly during a typical splicing cycle, and, importantly, "open" and "closed" forms of the spliceosome have been linked to changes in splicing fidelity (6, 14, 15). Cryptic splicing could result from local movements of the pre-mRNA within the catalytic core of the spliceosome while it is in an open form.

Here, we characterize two *prp-8* alleles identified in a *Caenorhabditis elegans* screen designed to select for factors that alter cryptic splicing frequency. Our data suggest that stabilization of a more open form of the spliceosome's catalytic core promotes cryptic splicing, and that cryptic splicing occurs independently of spliceosome selection between bona fide alternative sites, and by a different mechanism.

Results

Genetic Screen to Identify Alleles That Alter the Frequency of Cryptic Splicing. The *C. elegans* (worm) *unc-73* gene encodes a protein required for proper axon guidance and cell migration. The *unc-73(e936)* allele bears a G → U mutation at the first nucleotide of intron 15, which disrupts splicing and causes uncoordinated locomotion. We previously reported the use of *unc-73(e936)* in a genetic screen to identify cellular factors that alter cryptic splicing patterns (16). In this approach, *unc-73(e936) C. elegans*

Significance

The spliceosome selects, and in the case of alternative splicing, contextually distinguishes between, splice sites with extremely high fidelity. However, when a splice site becomes mutated, as in many human diseases, the spliceosome can aberrantly select nearby "cryptic" splice sites, which produce nonfunctional protein. It is unclear how the spliceosome routinely selects against cryptic sequences. Here, we implicate core components of the spliceosome itself in its ability to select against cryptic splice sites and show that how the spliceosome selects against cryptic splice sites is different than how it selects between bona fide splice sites during alternative splicing. In addition to providing insight into an essential cellular process, our work is relevant to the development of therapeutics that act by modulating splice-site choice.

Author contributions: M.M. and A.M.Z. designed research; M.M., S.Y., C.S., L.E.R., A.R., J.M.R., S.K., and A.M.Z. performed research; M.M., S.K., and A.M.Z. contributed new reagents/analytic tools; M.M., S.K., C.G., and A.M.Z. analyzed data; and M.M., C.G., and A.M.Z. wrote the paper.

Reviewers: M.B., University at Albany; and G.D., HHMI and University of Pennsylvania.

The authors declare no conflict of interest.

Data deposition: The data reported in this paper have been deposited in the Gene Expression Omnibus (GEO) database, https://www.ncbi.nlm.nih.gov/geo (accession no. GSE113275).

[1]Present address: Cardiovascular Institute, Stanford University, Stanford, CA 94305.

[2]To whom correspondence may be addressed. Email: christineguthrie@gmail.com or zahler@ucsc.edu.

This article contains supporting information online at www.pnas.org/lookup/suppl/doi:10.1073/pnas.1819020116/-/DCSupplemental.

Published online January 23, 2019.

are *N*-nitroso-*N*-ethylurea (ENU)-mutagenized and their F_2 progeny screened for improved locomotion. Changes in locomotion often result from mutations in splicing factors that promote changes in splice-site choice (Fig. 1*A*), improving locomotion through increasing the level of in-frame *unc-73* messages by promoting use of the wild-type 5′ SS (Fig. 1*B* and Table 1). No cryptically spliced *e936* transcripts are subject to nonsense-mediated decay.

We previously identified *az24*, a semidominant extragenic allele that altered cryptic-splicing frequency, but we had not identified the gene (16). By sequencing spliceosome genes in the 1.4-MB region of the genome to which we mapped *az24*, we identified G654E in the *C. elegans* homolog of Prp8 (PRP-8). To verify that *prp-8*(G654E) causes improved locomotion and changed cryptic splicing patterns seen in *az24*, we used CRISPR-cas9 to remake this mutation in wild-type worms and crossed this allele into the *unc-73(e936)* background (*SI Appendix*, Fig. S1). We call the CRISPR *prp-8*(G654E) allele *az29*. Both *az24* and *az29* improve worm locomotion, likely due to an increase in the frequency of in-frame splicing of the *unc-73(e936)* transcript (Fig. 1*B* and Table 1), leading to the production of more UNC-73 protein. We repeated the screen and identified a semidominant allele, *az43*, which mapped to *prp-8*(T524S). We used CRISPR-cas9 to generate *prp-8(az50)*, a T524S amino acid substitution (*SI Appendix*, Fig. S1) designed to validate *az43*. Both the *az43* and *az50* T524S alleles affect *e936* cryptic splice-site selection; they lead to increased usage of both the −1 and WT cryptic 5′ SS and lower the use of the +23 cryptic SS, increasing the abundance of mRNAs coding for full-length UNC-73 (Fig. 1*B* and Table 1).

Table 1. *prp-8* alleles promote use of wild-type 5′ SS

Genotype	+23, %	wt, %	−1, %
unc-73(e936);prp-8(+)	73.7	**14.8**	11.5
unc-73(e936);prp-8(+)	74.3	**13.5**	12.2
unc-73(e936);prp-8(az24) G654E	53.6	**24.2**	22.2
unc-73(e936);prp-8(az24) G654E	53.2	**23.1**	23.7
unc-73(e936);prp-8(az29) G654E	53.4	**27.0**	19.6
unc-73(e936);prp-8(az29) G654E	55.1	**25.7**	19.1
unc-73(e936);prp-8(az43) T524S	52.2	**28.3**	19.6
unc-73(e936);prp-8(az43) T524S	53.8	**28.4**	17.8
unc-73(e936);prp-8(az50) T524S	56.9	**26.3**	16.8
unc-73(e936);prp-8(az50) T524S	56.3	**25.0**	18.7

Relative usage of each of the cryptic splice-sites for *unc-73(e936)* intron 15 in the gel shown in Fig. 1*B*.

***prp-8* Alleles Map to Conserved Regions of PRP-8 That Surround and Stabilize Key Components of the Spliceosome's Catalytic Core.** Prp8 surrounds and stabilizes the spliceosome's catalytic core, directly contacting the catalytic U6 snRNA, pre-mRNA substrate, and the portion of U5 snRNA that positions the exons for ligation. It also makes extensive contacts with multiple spliceosomal proteins, including Snu114 (7, 9). *az24* and *az43 prp-8* alleles map to regions of Prp8's N-terminal domain that are highly conserved in both sequence and structure (Fig. 2), consistent with being important for spliceosome function.

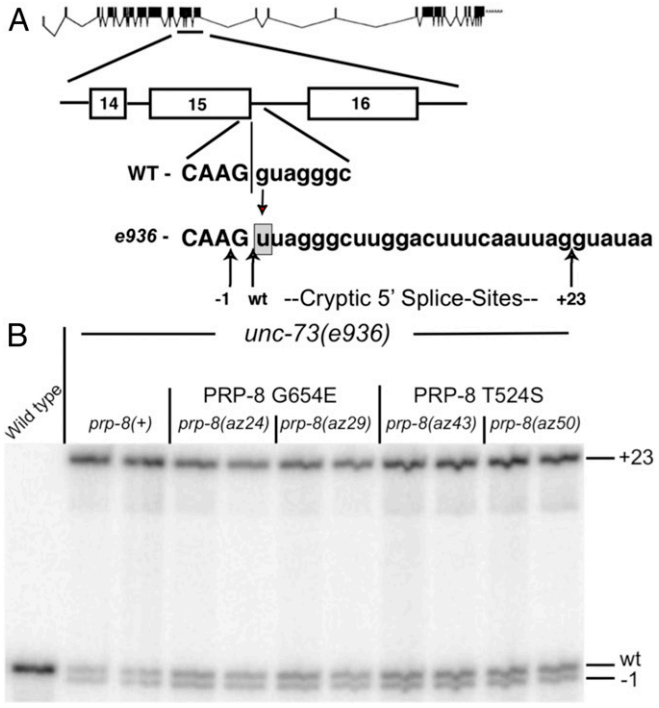

Fig. 1. Two suppressor alleles map to *prp-8*. (*A*) Exon structure of *unc-73* (32). The G → U substitution at the first base of intron 15 in the *e936* allele, along with the cryptic SS activated by it, (−1, wt, +23) are indicated. (*B*) ^{32}P-RT-PCR products from independent RNA extractions were separated on 6% polyacrylamide denaturing gels. Bands corresponding to use of the different cryptic SS indicated. Quantification presented in Table 1.

Analysis of available spliceosome structures suggests that the *az24* and *az43* alleles act by destabilizing the spliceosome's catalytic core. *az43* maps to PRP-8 amino acid T524. In structures of the *Saccharomyces* spliceosome, this amino acid (T607 in *S. cerevisiae* and T532 in humans) interacts with the phosphodiester backbone of the pre-mRNA intron's 5′ SS between the +2 and +3 positions (7, 8, 10). Thus, Prp8 serves as an additional contact stabilizing the 5′ SS within the spliceosome's catalytic core (Fig. 2 *C* and *D*). Substitution of Ser for Thr in *az43* removes a methyl group, decreasing the number of contacts supporting the 5′ SS.

The other allele, *az24* (G736E in *S. cerevisiae*), maps to a loop in Prp8's N-terminal domain (Fig. 2 *C* and *E*), which we refer to as the "740 loop." This loop is only resolved in structures of activated spliceosomes (*SI Appendix*, Fig. S2), suggesting it is stabilized after the spliceosome's catalytic core has closed (7, 9, 11, 17–19). The 740 loop braces the catalytic U6 snRNA internal stem loop, helping organize the spliceosome's catalytic core (Fig. 2*E*). Mutation of a Gly to a Glu adds negative charge in proximity to negatively charged U6 snRNA, potentially destabilizing the spliceosome's catalytic core.

Homologous *S. cerevisiae* prp8 Alleles Inform How Cryptic Splicing Frequency Is Altered. We created *S. cerevisiae* strains carrying homologous alleles to the *az24* and *az43 prp-8* alleles to take advantage of tools not available in *C. elegans*. We performed growth assays to determine whether *prp8* alleles impact *S. cerevisiae* growth and/or survival. We were able to recover *prp8-G736E(az24) S. cerevisiae*, indicating that *prp8-G736E(az24)* does not affect viability (Fig. 3*A*). We compared the growth of *prp8-G736E(az24)* to that of *PRP8*. The strains grew identically (Fig. 3*A*), indicating that *prp8-G736E(az24)* does not affect *S. cerevisiae* growth. Strikingly, though *az43 C. elegans* show no gross morphological phenotypes: *prp8-T607S(az43)* is lethal in *S. cerevisiae* (Fig. 3*B*). Given that worm 5′ SS are more degenerate, it is surprising that removal of a 5′ SS backbone-stabilizing interaction would have a stronger effect in yeast. One explanation is that Prp8-T607S spliceosomes splice less efficiently due to problems stabilizing pre-mRNA. Because most *S. cerevisiae* introns are in essential transcripts, decreased efficiency may not be tolerable.

We used the well-characterized Act-Cup reporter to assess how *S. cerevisiae prp8* alleles interact with different SS variants. In this system, the *ACT1* intron has been fused to the copper

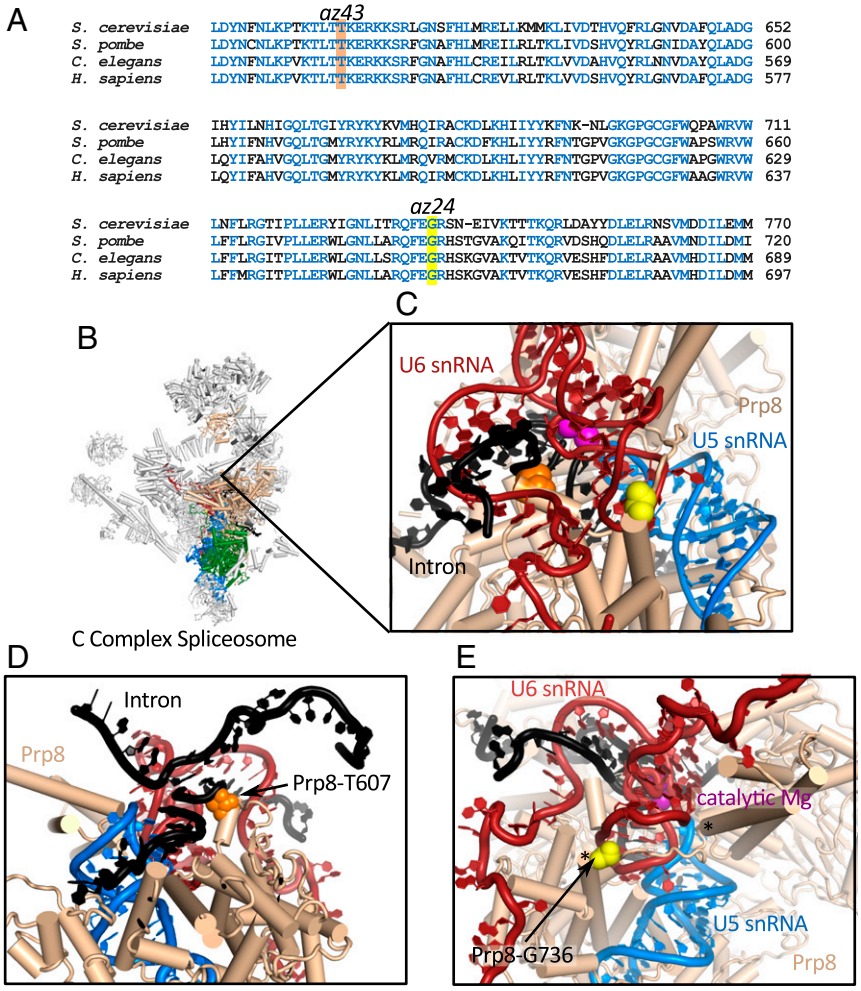

Fig. 2. *prp-8* alleles map to conserved regions of Prp8. (*A*) ClustalOmega (33) alignment of Prp8 sequences showing conservation (blue) in the region of *az24* (yellow) and *az43* (orange). (*B*) *S. cerevisiae* C complex structure (5LJ3) (7) highlighting Prp8's (tan) central position, Snu114 (green), U5 snRNA (blue), and U6 snRNA (red). These interactions are virtually identical in all post B-complex structures. (*C*) Zoom to spliceosome's catalytic core. Catalytic Mg^{2+}, magenta. Positions of Prp8-T607 (orange) and Prp8-G736 (yellow) are shown. (*D*) Prp8-T607 (orange) contacts the intron (black) 5′ SS +3 phosphate. (*E*) Prp8-G736 (yellow) is part of a structured loop (edges indicated by asterisks) that forms during activation. This loop acts as a brace, supporting U6 snRNA.

detoxification protein *CUP1*, such that levels of *CUP1* mRNA transcript and, thus, levels of Cup1 protein, are dependent upon splicing efficiency, which can be directly inferred by monitoring the growth of *S. cerevisiae* on copper-containing media (20). *PRP8* and *prp8-G736E(az24) S. cerevisiae* were transformed with Act-Cup reporters (Fig. 3*C*), and the ability of *prp8-G736E* to splice these reporters was determined. We saw no change in general splicing efficiency, as indicated by the WT splicing reporter. The G5A reporter, which introduces a G → A substitution at position five of the 5′ SS, was the only reporter tested where *prp8-G736E* exhibited a phenotype (Fig. 3*C*). The negative effect on growth was slight but repeatable, consistent with RT-qPCR data showing a modest but not statistically significant decrease in the level of *prp8-G736E* G5A Act-Cup mRNA (*SI Appendix*, Fig. S3). The G5A 5′ SS mutation loosens contacts between pre-mRNA and the spliceosome, and a previously published *prp8* allele implicated in spliceosome catalytic core stability is particularly sensitive to G5A (13). Together these data implicate Prp8 in the stability of the spliceosome's catalytic core.

To gain more insight into the mechanisms underlying how Prp8 impacts cryptic SS selection, we used comparative growth assays to search for genetic interactions between *prp8-G736E* and other core spliceosome components implicated in catalytic core. We identified a genetic interaction between *prp8-G736E* and *snu114-12*. Snu114 is a GTPase that has homology with ribosomal translocation factor EF-G. Its GTPase activity correlates with several important steps in spliceosome assembly, catalysis, and disassembly (21). Snu114 physically and genetically interacts with Prp8 (22). The *snu114-12* allele was designed to decrease Snu114's rate of GTP hydrolysis and is temperature sensitive (22). *prp8-G736E* suppresses *snu114-12* temperature sensitivity. *prp8-G736E snu114-12* also exhibits cold sensitivity, a phenotype not present independently in *prp8-G736E* or *snu114-12* (Fig. 3*D* and *SI Appendix*, Fig. S4). Together these data implicate Prp8 regulation by Snu114 in suppression of cryptic splicing.

Multiple *C. elegans* PRP-8 Amino Acid Substitutions at Position 654 Are Viable and Suppress Cryptic Splicing. *C. elegans* PRP-8 amino acid G654 maps to the 740 loop, a region of PRP-8 that is unstructured during early assembly but later structures and interacts with the catalytic U6 internal stem loop (Fig. 2*E* and *SI Appendix*, Fig. S2). This intriguing structural transition, coupled with our yeast data, led us to test whether any additional amino acid substitutions at G654 are viable in *C. elegans*, and if such substitutions can also suppress cryptic splicing. To do this, we performed CRISPR mutagenesis. We used a 100-nt *prp-8* repair

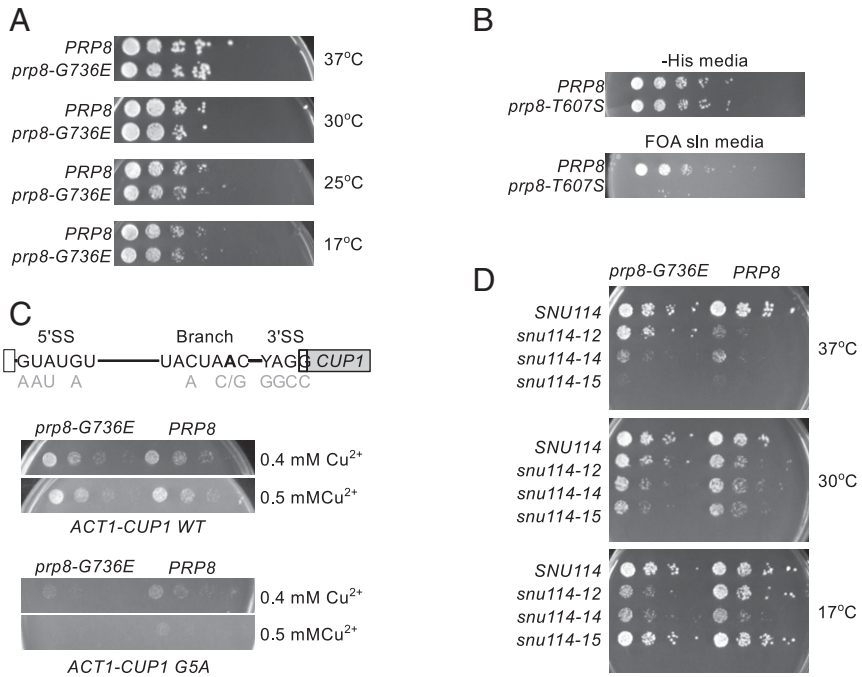

Fig. 3. Effects of *S. cerevisiae prp8* alleles. (*A*) *prp8-G736E* grows identically to wild-type *S. cerevisiae*. (*B*) FOA selection shows that, in the absence of wild-type *PRP8*, *prp8-T607S* is lethal. (*C*) Act-Cup analyses. (*Top*) Act-Cup reporter showing all intron substitutions. (*Middle*) *prp8-G736E* grows as *PRP8* when challenged with a WT reporter. (*Bottom*) *prp8-G736E* growth on copper-containing media is compromised by G5A. (*D*) *prp8-G736E* exacerbates *snu114-12* cold sensitivity while suppressing temperature sensitivity.

oligonucleotide in which we substituted the G654 codon with three Ns to template random codons (*SI Appendix*, Fig. S5*A*). We recovered K, R, L, I, V, P, C, and E substitutions at position G654, as well as an 8-aa insertion, TKRRKSPS, between amino acids F652 and E653 (*SI Appendix*, Fig. S5*B*). All CRISPR mutant worms appear healthy, and no new recessive lethal alleles were recovered.

We crossed these alleles with *unc-73(e936)* to determine their effects on cryptic splicing frequency (Table 2). All CRISPR-generated *prp-8* alleles showed changes in cryptic SS choice, increasing use of the WT *unc-73(e936)* exon 15 SS, although none to the same extent as the original G654E allele. Consistent with this molecular phenotype, using thrashing assays, a common assay of worm locomotion, we observed suppression of the *unc* phenotype to a degree consistent with the change in cryptic SS choice. The 8-aa 740 loop insertion allele also shows suppression at both the molecular and organismal level (Table 2). Together these data show that a wide variety of amino acids are tolerated at position G654 in *C. elegans*. We hypothesize that these changes to cryptic SS selection result from destabilization of the Prp8 740 loop.

Only Thr, Ser, and Val Can Be Tolerated at Position 524 in *C. elegans*. We performed CRISPR-*cas9* random mutagenesis experiments to produce the full range of possible T524 amino acid substitutions (*SI Appendix*, Fig. S5*C*). We recovered only T, S, and V as viable T524 substitutions (*SI Appendix*, Fig. S5*D*). Recovery of Thr and Ser are not surprising given that these are the wild type and the viable *az43* alleles identified in our forward genetic screen. To test whether the T524V substitution in PRP-8 could also impact cryptic splicing frequency, we used genetic crosses to construct *unc-73(e936); prp-8(T524V)* animals. These double mutant animals were uncoordinated (no phenotypic suppression), slow to mature, and had few to no progeny, making it

Table 2. Cryptic splicing measurements of the *unc-73(e936)* gene in the presence of the PRP-8 G654 substitution alleles

Strain	Genotype	PRP-8	"+23", %	wt, %	"−1", %	Thrashes/min
SZ181	*unc-73(e936); prp-8(+)*	wt	72.9, 73.7	12.1, 13.8	14.9, 12.5	10.2 ± 2.9
SZ155	*unc-73(e936); prp-8(az29)*	G654E	54.3, 53.7	27.1, 24.9	18.6, 21.4	108.4 ± 9.9
SZ255	*unc-73(e936); prp-8(az75)*	G654K	64.5, 62.6	19.5, 19.7	16.0, 17.7	50.8 ± 8.0
SZ256	*unc-73(e936); prp-8(az76)*	G654L	56.7, 56.5	22.5, 23.7	20.8, 19.7	59.8 ± 12.7
SZ257	*unc-73(e936); prp-8(az77)*	G654P	63.4, 62.0	20.1, 21.8	16.6, 16.2	41.4 ± 8.8
SZ258	*unc-73(e936); prp-8(az79)*	G654I	59.3, 59.4	21.7, 21.8	19.0, 18.8	40.6 ± 10.1
SZ259	*unc-73(e936); prp-8(az80)*	G654C	65.8, 62.6	20.4, 20.6	13.8, 16.7	33.4 ± 5.9
SZ260	*unc-73(e936); prp-8(az82)*	G654V	57.4, 57.4	23.3, 23.3	19.3, 19.3	43.8 ± 5.5
SZ261	*unc-73(e936); prp-8(az83)*	8aa ins.	62.9,61.7	21.7, 23.4	15.4, 14.9	85.8 ± 15.9
N2	*unc-73(+); prp-8(+)*	wt		100.0		133.4 ± 11.1

The last column is a thrash assay in which L4 worms were placed in a drop of M9 medium on a glass slide and the number of times that they bent their body across the central axis in 1 min was measured. Mean and SD of 10 independent trials listed.

Table 3. Pairwise comparison sums of MISO analysis of alternative splicing changes

pairSum	Alt 5′ splice-site events	Alt 3′ splice-site events	Alt cassette exons
PRP-8 G654E - Max pairwise comparison sum = 8			
8	0/3	0/1	0/1
7	0/3	0/1	0/0
6	**2**/11	0/16	0/0
PRP-8 T524S - Max pairwise comparison sum = 12			
12	0/0	**2**/3	0/0
11	0/3	**2**/3	0/0
10	**3**/10	0/0	**1**/2
9	0/2	**6**/10	0/2

Number of potential events after inspection/number of potential initially flagged events. The bold column in the table represents the percentage of in-frame *unc-73* messages in the animals.

impossible to recover RNA for testing, unlike T524S *C. elegans*, which appear as wild type.

One striking observation from this CRISPR-based mutagenesis at T524 is that in the F_1 progeny of the CRISPR-cas9 injected parents, we saw many dead and dying embryos and early-stage larvae. This is a phenomenon that we had not seen previously, and we did not observe any substitutions of T524 that were viable as heterozygotes but homozygous lethal. These results point to the possibility that other amino acid substitutions at T524 besides Ser and Val produce a dominant lethal form of PRP-8.

***prp-8* Alleles Do Not Dramatically Impact Normal Alternative Splicing Patterns.** To determine whether *prp-8* alleles promote global changes in alternative splicing of native genes, we performed high-throughput strand-specific mRNA sequencing of 100-nt paired-end reads generated from *prp-8 C. elegans* (*SI Appendix*, Table S1). We looked for changes in alternative splicing between libraries. We created de novo a dataset of alternative 5′ SS events, alternative 3′ SS events, and alternative cassette exon events. We next used MISO (23) to do pairwise comparisons for each SS choice event, comparing strains carrying the *unc-73 (e936)* mutation against those with both *unc-73(e936)* and a *prp-8* allele. Events in which MISO detected a change in percent spliced in (ΔPSI) ≥ 0.20 in each comparison (a change of ≥20%) were ranked by a total number of pairwise comparisons in which significant changes occurred (Table 3). This sum of significant changes for an event across all pairwise comparisons is the pairwise comparison sum, or pairSum. Table 3 shows the number of alternative splicing events detected for each pairSum for worms carrying each of the two *prp-8* mutant alleles. We examined Sashimi plots for each flagged event along with BAM tracks to visually confirm them (Table 3) (23). The majority of events that passed visual confirmation were validated by ^{32}P-RT-PCR (*SI Appendix*, Fig. S5).

Data from *prp-8(*G654E) worms indicated only two alternative 5′ splicing events (T12C9.7 and *stip-1*) (Table 4 and *SI Appendix*, Fig. S5 *A* and *B*). For the *prp-8*(T524S) mutant worms, we identified three alternative 5′ SS events, one alternative cassette exon event, as well as 10 alternative 3′ SS events (Table 5 and *SI Appendix*, Fig. S5 and Table S2). *prp-8* T524S mutant altered 5′ SS usage for T12C9.7 in the opposite direction of G654E (Table 4 and *SI Appendix*, Fig. S5*A*). The five strongest changes in alternative 3′ SS in *prp-8(T524S)* worms were confirmed by ^{32}P-RT-qPCR, without an obvious bias toward the upstream or downstream 3′ SS (Table 5 and *SI Appendix*, Fig. S5 *C–G*). Alternative 3′ SS choice events promoted by the *prp-8* T524S mutation were unchanged or only minimally changed by the *prp-8* G654E mutation, indicating these alleles have distinct effects on 3′ SS usage (Table 5 and *SI Appendix*, Fig. S5). We hypothesize

Table 4. Alternative splicing events predicted from *prp-8 G654E* mRNA-Seq analysis

Genotype	Up 5′SS use str. 1,2, %
Gene & Sequence: T12C9.7; TTTATTTCTG▲GTT△gtgagaatttgttttatagttt	
snrp-27(+); prp-8(+)	18.65, 18.74
snrp-27(M141T); prp-8(+)	97.55, 95.55
snrp-27(+); prp-8(G654E)	35.61, 35.83
snrp-27(+); prp-8(T524S)	1.41, 1.12
Gene & Sequence: *stip-1*; AGGATCAGGCGACATAT G▲ GTGGG△gtgagatcattgaaaa	
snrp-27(+); prp-8(+)	75.96, 75.74
snrp-27(M141T); prp-8(+)	94.46, 95.54
snrp-27(+); prp-8(G654E)	92.63, 91.88
snrp-27(+); prp-8(T524S)	86.61, 87.07
Gene & Sequence: *spat-2;* AACAGCGTT△GTGAGG ATGGCCTTGCAAGAAGGG▲gtgcgggctta	
snrp-27(+); prp-8(+)	71.76, 72.07
snrp-27(M141T); prp-8(+)	45.43, 42.86
snrp-27(+); prp-8(G654E)	59.26, 61.84
snrp-27(+); prp-8(T524S)	50.34, 51.64

Sequences of the alternative spliced regions. 5′ SSs promoted in *prp-8* mutant indicated by a filled triangle, partner 5′ SS indicated by an open triangle. Uppercase are sequences that can be exons; lowercase are always intronic. Below the sequence is quantitation of alternative 5′ splice-site usage by ^{32}P-RT-PCR analysis. Genotypes are indicated. T12C9.7 was identified in the *prp-8* G654E library, *stip-1* in both *prp-8* libraries, and *spat-2* in the *prp8* T524S library.

Table 5. Analysis of alternative 3′ splicing events predicted from mRNA-Seq analysis of the prp-8 T524S mutant libraries

Genotype	Up 3′ SS use strain 1,2, %
Gene & Sequence: *cdt-2* aaatcaaaaag▲ATTTCAG△TTTTTCCCGC	
prp-8(+)	18.24, 18.41
prp-8(G654E)	27.65, 28.28
prp-8(T524S)	51.51, 52.45
Gene & Sequence: T10E9.14 atattttgcag△TTTCAG▲GAAACTATCAAC	
prp-8(+)	16.76, 17.72
prp-8(G654E)	19.34, 20.04
prp-8(T524S)	5.44, 4.58
Gene & Sequence: F48D4.6 gttattcag▲TGTTCCAG△AAACAG△TGACGACTT	
prp-8(+)	54.90, 53.69
prp-8(G654E)	49.98, 51.13
prp-8(T524S)	79.53, 79.69
Gene & Sequence: W09G3.7 atcacgaatttag△CTTCCAG▲ATCGGTGGT	
prp-8(+)	84.59, 83.27
prp-8(G654E)	81.61, 81.82
prp-8(T524S)	62.01, 60.82
Gene & Sequence: *dct-1* aacgcttcag△GTATGTCAG▲AATCGTGGGTGGAA	
prp-8(+)	62.48, 56.68
prp-8(G654E)	48.90, 50.14
prp-8(T524S)	44.33, 45.60

Five of the 10 alternative 3′ splicing events were tested. Sequences of the alternatively spliced regions are shown, with the 3′ SSs promoted in the *prp-8* mutant indicated by a filled triangle, and the partner 3′ SS by an open triangle (in F48D6.4 there are three alternative 3′ SSs). Uppercase indicates sequences that can be exons, while lowercase are always intronic. Below the sequence is quantitation of relative alternative 3′ SS usage by ^{32}P-RT-PCR analysis (*SI Appendix*, Fig. S5). Genotypes are indicated.

that the changes in 3′ SS selection may be a consequence of altered interactions between Prp8 and the pre-mRNA branchpoint.

We are confident in our analysis pipeline as this methodology previously yielded 26 high-confidence alternative splicing events for the *snrp-27(az26)* allele (24). While the *snrp-27* and two *prp-8* alleles have almost identical effects on *unc-73(e936)* cryptic 5′ SS choice, our sequencing analysis indicates that they can have differential effects on alternative splicing, suggesting that they may operate at distinct stages of splicing. In contrast to our previous studies, the small number of alternative splicing events that we observe suggest that these *prp-8* mutations do not cause strong global changes in alternative splicing. We conclude that the *prp-8* alleles lead to a small number of confirmable changes in the usage of SSs located in close proximity to each other (i.e., that look like cryptic sites), consistent with the spliceosome being in a more open conformation that may allow slippage between juxtaposed SSs.

Discussion

The remarkable number of high-resolution structures available paint a very clear picture of the relative conformations of the spliceosome's catalytic core at multiple stages of the splicing cycle. These data illustrate how the spliceosome reorients during activation to close its catalytic core. However, such data present only static images of what is known to be an incredibly dynamic molecular machine. The spliceosome's catalytic core is dynamic, changing its conformation from open to closed forms repeatedly during a typical splicing cycle (Fig. 4 *A* and *B*). Such dynamics are required to position pre-mRNA for catalysis, and spliceosome dynamics may be linked to high-fidelity splicing (6, 13, 14, 25).

Here, we present our analysis of two *prp-8* alleles that alter the frequency of cryptic splicing in *C. elegans*. We show that improvement of *unc-73(e936)* locomotion is an exquisitely sensitive tool for identifying cellular factors involved in cryptic SS selection that act through a variety of mechanisms. Using a combination of structural and genetic approaches in *S. cerevisiae*, we suggest that these *prp-8* alleles modulate cryptic splicing by negatively impacting catalytic core closure and/or stability during splicing (Fig. 4*C*). This may allow for cryptic SS to occupy the active site of the spliceosome even after initial definition of the 5′ SS. In the case of *unc-73(e936)*, a less stable catalytic core allows an intron beginning with a nonconsensus U more frequent access to the spliceosome's catalytic core, leading to an increase in in-frame messages and improved worm locomotion. We show that the *prp-8* alleles identified in our screen only impact cryptic splicing and can promote small alterations in the ratio of alternative splicing for a small number of juxtaposed alternative 5′ or

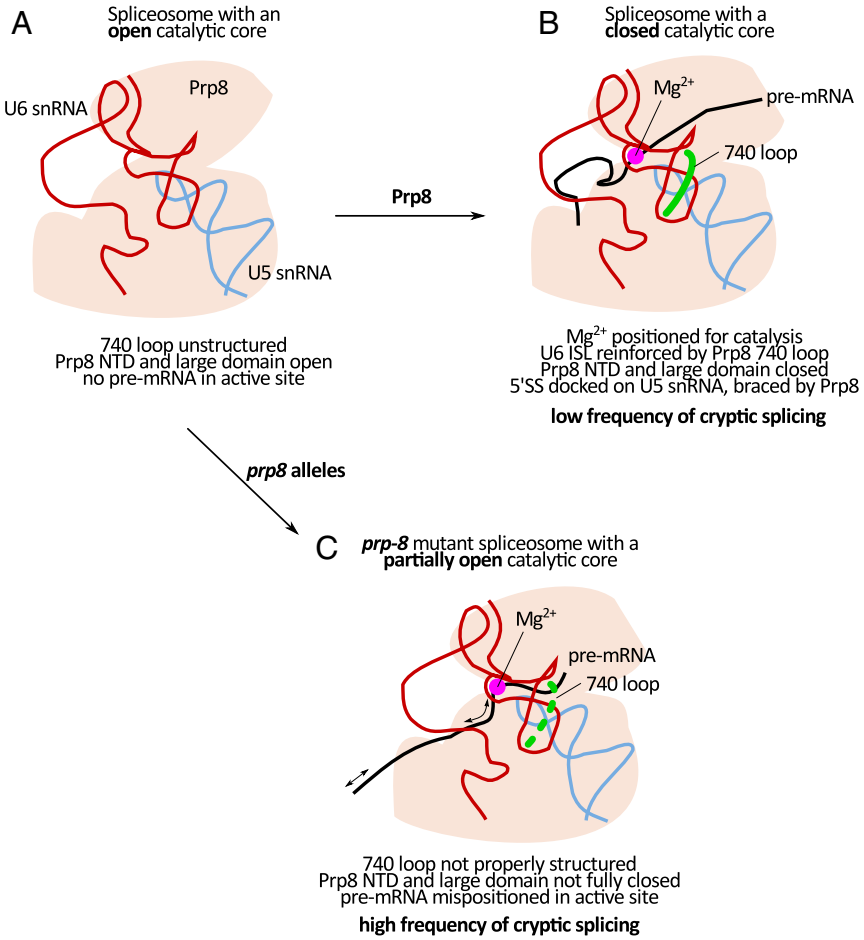

Fig. 4. Model. The spliceosome's catalytic core can be found in both open and closed conformations. Prp8 is shown (tan blob) with the 740 loop (green), U6 snRNA (red), U5 snRNA (blue), pre-mRNA (black), and Mg^{2+} (magenta). (*A*) When the catalytic core is open, there is no pre-mRNA docked to U5 snRNA, catalytic Mg^{2+} are absent, and the 740 loop is unresolved. (*B*) Upon closure, the large domain of Prp8 rotates with respect to the Prp8 NTD (top of Prp8 moves toward bottom). The Prp8 740 loop forms and is resolved by cryoEM (*SI Appendix*, Fig. S2). The 740 loop supports the U6 internal stem loop, which when in a closed conformation, coordinates Mg^{2+}. Pre-mRNA base pairs with the U5 snRNA. (*C*) We hypothesize *prp-8* alleles negatively affect closure, disrupting pre-mRNA positioning and the 740 loop. *prp8* spliceosomes would allow movement of pre-mRNA within their catalytic core, which could result in cryptic splicing.

3′ SS, but do not have global effects on alternative splicing. Together, our data directly link Prp8-mediated alteration of the spliceosome's catalytic core to cryptic splicing. More tests are needed to address whether other methods of changing the spliceosome's catalytic core also lead to changes in cryptic splicing, or if this mechanism is unique to Prp8. That *prp-8* alleles do not greatly impact alternative splicing suggests that Prp8's role in cryptic SS choice occurs independently of exon and/or intron definition, and that it likely occurs via a distinct mechanism.

Materials and Methods

Screen Design and Identification of Alleles That Alter Cryptic Splicing Frequency. The ENU genetic screen to identify alleles of *unc-73(e936)* was adapted from a suppressor screen as described (16). *az24* was isolated but not identified in ref. 16; *az43* was identified in recent repeats of that screen.

CRISPR Mutagenesis. CRISPR Cas9-directed mutagenesis to generate *az29, az50*, and T524 and G654 randomization alleles was performed using a co-CRISPR protocol as described (24). *prp-8* repair oligos are described in *SI Appendix*, Table S3. Restriction digests of PCR products were used to track mutations (24, 26).

^{32}P-RT-qPCR Analysis. Starting with 4 μg of total mixed stage RNA, reverse transcription was performed (24). Primers are indicated in *SI Appendix*, Table S4. After 25–30 extension cycles (95 °C for 0.5 min, 59 °C for 0.5 min, 68 °C for 0.5 min), PCR products were recovered by phenol:$CHCl_3$ extraction and ethanol precipitation. Ethanol precipitates were resuspended in 20 μL of formamide and 2 μL were separated on a 6% polyacrylamide urea TBE denaturing gel. Products were visualized with a Molecular Dynamics Typhoon PhosphorImager and quantified by ImageQuant (GE Healthcare Life Sciences).

***S. cerevisiae* Strain Construction and Growth Assays.** yMeg030 (Mat α prp8::LYS cup1::ura3-52 his leu lyse ura ade yCP50-PRP8), yMeg035 (MAT a prp8::LYS his leu lys ura yCP50/PRP8), and yTB108 (MAT α prp8::LYS snu114:KanMX6 his leu lys trp ura yCP50/PRP8 pRS316-SNU114) have been described (22, 27). pRS313-prp8-G736E was created using QuikChange. pRS313-prp8-T607S was created by gap repair of a synthesized fragment containing the T607S mutation (28). Plasmids are available from Addgene. Mutant strains were created by 5FOA shuffling (28). Growth assays were performed by serially diluting log phase cultures grown in rich media and spotting onto rich media. Growth was assessed at 37 °C (2 d), 30 °C (2 d), 25 °C (4 d), or 17 °C (6 d).

ACT-CUP Reporter Analyses. *PRP8* or *prp8-G736E S. cerevisiae* transformed with an Act-Cup reporter plasmid were grown as described (20, 28). Growth was assessed after 3 d at 30 °C. RT-qPCR analysis was performed with total RNA isolated by the hot phenol method from Act-Cup reporter strains. Specific primers used for qPCR have been described (13).

RNA-Seq Sample Preparation and Analysis. RNA was isolated for library construction from mixed stage populations of *C. elegans* (September 2017 preps) or populations enriched for young adults (May 2016 preps) as described (24). FASTQ files and processed .gtf files are in Gene Expression Omnibus accession no. GSE113275. Two libraries from two independent RNA isolations were prepared per strain. Sequences trimmed to 80 bases were mapped to the *C. elegans* genome using STAR (29). We used a custom script to de novo identify all alternative 5′ SS and 3′ SS events separated by ≦ 50 nt (30) and AltEventFinder (31) to identify cassette exon alternative splicing events. We used MISO (23) to do pairwise comparisons of these libraries for all alternative splicing events. Events in which MISO detected a change in PSI of ≥0.20 were ranked by the total number of pairwise comparisons in which significant changes occurred. The sum of significant changes for an event across all pairwise comparisons is the pairSum. The delta PSI cutoff of 0.20 was chosen because of our previous experience and the issue of false flags that require individual inspection (Table 3) (24). A minimum change in alternative SS usage of 20% allowed us to separate true changes in alternative splicing. This approach may miss some subtle alternative splicing changes, but there is not a widespread destabilization of alternative SS selection.

ACKNOWLEDGMENTS. We thank Sam Gu and Zhouli Ni of Rutgers University for help in getting the A.M.Z. laboratory started on CRISPR experiments in *C. elegans*; Manny Ares and Naomi Tesfuzigta for the idea for a single-site oligonucleotide-directed homologous repair genetic randomization experiment; Surabhi Jain and Ken Osterhoudt for help in genetic screening; Magda Konarska for key Prp8 cloning advice; and M. Jurica, A. de Bruyn Kops, M. Konarska, J. Arribere, and H. Madhani for helpful conversations. M.M. and C.G. were supported by the Agouron Institute and National Institute of General Medical Sciences Grant R01GM2119. C.G. is an American Cancer Society Research Professor of Molecular Genetics. Research in the A.M.Z. laboratory is supported by National Science Foundation Grant MCB-1613867. L.E.R. was a fellow of the University of California, Santa Cruz (UCSC) Postbaccalaureate Research Education Program (R25GM104552) funded by the NIH. A.R. is a fellow of the UCSC Initiative for Maximizing Student Diversity Program (R25GM058903).

1. Will CL, Lührmann R (2011) Spliceosome structure and function. *Cold Spring Harb Perspect Biol* 3:a003707.
2. Singh RK, Cooper TA (2012) Pre-mRNA splicing in disease and therapeutics. *Trends Mol Med* 18:472–482.
3. Cvačková Z, Matějů D, Staněk D (2014) Retinitis pigmentosa mutations of SNRNP200 enhance cryptic splice-site recognition. *Hum Mutat* 35:308–317.
4. Semlow DR, Blanco MR, Walter NG, Staley JP (2016) Spliceosomal DEAH-box ATPases remodel pre-mRNA to activate alternative splice sites. *Cell* 164:985–998.
5. Tang Q, et al. (2016) SF3B1/Hsh155 HEAT motif mutations affect interaction with the spliceosomal ATPase Prp5, resulting in altered branch site selectivity in pre-mRNA splicing. *Genes Dev* 30:2710–2723.
6. Mayerle M, et al. (2017) Structural toggle in the RNaseH domain of Prp8 helps balance splicing fidelity and catalytic efficiency. *Proc Natl Acad Sci USA* 114:4739–4744.
7. Galej WP, et al. (2016) Cryo-EM structure of the spliceosome immediately after branching. *Nature* 537:197–201.
8. Zhan X, Yan C, Zhang X, Lei J, Shi Y (2018) Structure of a human catalytic step I spliceosome. *Science* 359:537–545.
9. Yan C, Wan R, Bai R, Huang G, Shi Y (2016) Structure of a yeast activated spliceosome at 3.5 Å resolution. *Science* 353:904–911.
10. Bertram K, et al. (2017) Cryo-EM structure of a human spliceosome activated for step 2 of splicing. *Nature* 542:318–323.
11. Plaschka C, Lin P-C, Nagai K (2017) Structure of a pre-catalytic spliceosome. *Nature* 546:617–621.
12. Haselbach D, et al. (2018) Structure and conformational dynamics of the human spliceosomal B^{act} complex. *Cell* 172:454–464.e11.
13. MacRae AJ, et al. (2018) Prp8 positioning of U5 snRNA is linked to 5′ splice site recognition. *RNA* 24:769–777.
14. Query CC, Konarska MM (2004) Suppression of multiple substrate mutations by spliceosomal prp8 alleles suggests functional correlations with ribosomal ambiguity mutants. *Mol Cell* 14:343–354.
15. Liu L, Query CC, Konarska MM (2007) Opposing classes of prp8 alleles modulate the transition between the catalytic steps of pre-mRNA splicing. *Nat Struct Mol Biol* 14:519–526.
16. Dassah M, Patzek S, Hunt VM, Medina PE, Zahler AM (2009) A genetic screen for suppressors of a mutated 5′ splice site identifies factors associated with later steps of spliceosome assembly. *Genetics* 182:725–734.
17. Nguyen THD, et al. (2016) Cryo-EM structure of the yeast U4/U6.U5 tri-snRNP at 3.7 Å resolution. *Nature* 530:298–302.
18. Fica SM, et al. (2017) Structure of a spliceosome remodelled for exon ligation. *Nature* 542:377–380.
19. Bai R, Yan C, Wan R, Lei J, Shi Y (2017) Structure of the post-catalytic spliceosome from Saccharomyces cerevisiae. *Cell* 171:1589–1598.e8.
20. Lesser CF, Guthrie C (1993) Mutational analysis of pre-mRNA splicing in Saccharomyces cerevisiae using a sensitive new reporter gene, CUP1. *Genetics* 133:851–863.
21. Bartels C, Urlaub H, Luhrmann R, Fabrizio P (2003) Mutagenesis suggests several roles of Snu114p in pre-mRNA splicing. *J Biol Chem* 278:28324–28334.
22. Brenner TJ, Guthrie C (2005) Genetic analysis reveals a role for the C terminus of the Saccharomyces cerevisiae GTPase Snu114 during spliceosome activation. *Genetics* 170:1063–1080.
23. Katz Y, et al. (2015) Quantitative visualization of alternative exon expression from RNA-seq data. *Bioinformatics* 31:2400–2402.
24. Zahler AM, et al. (2018) SNRP-27, the C. elegans homolog of the tri-snRNP 27K protein, has a role in 5′ splice site positioning in the spliceosome. *RNA* 24:1314–1325.
25. Anokhina M, et al. (2013) RNA structure analysis of human spliceosomes reveals a compact 3D arrangement of snRNAs at the catalytic core. *EMBO J* 32:2804–2818.
26. Paix A, Schmidt H, Seydoux G (2016) Cas9-assisted recombineering in C. elegans: Genome editing using in vivo assembly of linear DNAs. *Nucleic Acids Res* 44:e128.
27. Mayerle M, Guthrie C (2016) Prp8 retinitis pigmentosa mutants cause defects in the transition between the catalytic steps of splicing. *RNA* 22:793–809.
28. Guthrie C, Fink GR (2004) *Guide to Yeast Genetics and Molecular and Cell Biology* (Gulf Professional Publishing, Houston).
29. Dobin A, et al. (2013) STAR: Ultrafast universal RNA-seq aligner. *Bioinformatics* 29:15–21.
30. Ragle JM, Katzman S, Akers TF, Barberan-Soler S, Zahler AM (2015) Coordinated tissue-specific regulation of adjacent alternative 3′ splice sites in C. elegans. *Genome Res* 25:982–994.
31. Zhou A, et al. (2012) Alt event finder: A tool for extracting alternative splicing events from RNA-seq data. *BMC Genomics* 13(Suppl 8):S10.
32. Steven R, et al. (1998) UNC-73 activates the Rac GTPase and is required for cell and growth cone migrations in C. elegans. *Cell* 92:785–795.
33. Li W, et al. (2015) The EMBL-EBI bioinformatics web and programmatic tools framework. *Nucleic Acids Res* 43:W580–W584.